

Realistic Simulations of Proton Transport along the Gramicidin Channel: Demonstrating the Importance of Solvation Effects

Sonja Braun-Sand, Anton Burykin, Zhen Tao Chu, and Arieh Warshel*

University of Southern California, 3620 South McClintock Avenue, SGM 418, Los Angeles, California 90089

Received: July 30, 2004; In Final Form: October 12, 2004

The nature of proton transduction (PTR) through a file of water molecules, along the gramicidin A (gA) channel, has long been considered as being highly relevant to PTR in biological systems. Previous attempts to model this process implied that the so-called Grothuss mechanism and the corresponding orientation of the water file plays a major role. The present work reexamines the PTR in gA by combining a fully microscopic empirical valence bond (EVB) model and a recently developed simplified EVB-based model with Langevin dynamics (LD) simulations. The full model is used first to evaluate the free energy profile for a stepwise PTR process. The corresponding results are then used to construct the effective potential of the simplified EVB. This later model is then used in Langevin dynamics simulations, taking into account the correct physics of possible concerted motions and the effect of the solvent reorganization. The simulations reproduce the observed experimental trend and lead to a picture that is quite different from that assumed previously. It is found that the PTR in gA is controlled by the change in solvation energy of the transferred proton along the channel axis. Although the time dependent electrostatic fluctuations of the channel and water dipoles play their usual role in modulating the proton-transfer process (*Proc. Natl. Acad. Sci. U.S.A.* **1984**, *81*, 444),¹ the PTR rate is mainly determined by the free energy profile. Furthermore, the energetics of the reorientation of the *unprotonated* water file do not appear to provide a consistent way of assessing the activation barrier for the PTR process. It seems to us that in the case of gA, and probably other systems with significant electrostatic barriers for the transfer of the proton charge, the PTR rate is controlled by the electrostatic barrier. This finding has clear consequences with regards to PTR processes in biological systems.

I. Introduction

Proton translocations (PTRs) play a major role in biochemistry in general and bioenergetics in particular.^{2–6} Prominent examples are the function of ATPase,⁷ bacteriorhodopsin,^{8–11} cytochrome *c* oxidase,^{12,13} and other biological systems. In view of the crucial role of biological PTR processes, it is important to gain a quantitative molecular understanding of the factors that control such processes.

Most attempts to describe biological PTR followed the initial picture of Nagle and co-workers^{14,15} and assumed that PTR in biological systems can be described as a concerted transfer across a “proton wire” where the key control is provided by the orientation of the elements that constitute the wire. Furthermore, several influential simulation studies^{16–18} have provided support to Nagle’s view and strengthen the feeling that PTR is fundamentally different than the transport of other ions and that the so-called Grothuss mechanism, that controls PTR in water, is the key to the control of biological PTR processes. This amounts to at least the implicit assumption that the effective barrier is controlled by water orientation (see below).

Another view of the factors that control biological PTR^{19–21} has been advanced on the basis of microscopic studies of proton transport in proteins.^{22,23} This view postulated that biological PTR is controlled by the electrostatic energy of the proton in different sites along the transport path.

The wide acceptance of the orientational control picture^{14,15,24–32} has been reassessed in recent studies of the water/proton

selectivity in aquaporin, which have started to recognize the importance of the electrostatic barrier.^{33–35} These studies have pointed out the important role of the electrostatic barrier and its role in biological PTR processes. However, some controversy remains with regard to the role of the Grothuss mechanism and the implication that this mechanism should be important in other systems.^{33–35}

A primary system where it has been assumed that the Grothuss mechanism plays a major role in the PTR process is the gramicidin A (gA) channel. Studies of this system have implied that the PTR through a water file is controlled by orientational effects of the water (see below). However, in view of the paradigm shift that emerged from the studies of aquaporin, it is important to reexamine the PTR in gA.

The present work uses the empirical valence bond (EVB) method^{23,36} (which is arguably the most effective current way of examining PTR in complex systems) and simulates the free energy profile of the PTR in gA. The time dependence of this process is then simulated by a recently introduced simplified version of the EVB model. It is found that the PTR in gA is controlled by the electrostatic energy of the transferred proton rather than by the Grothuss mechanism.

II. Methods

Our goal is to conduct a reliable study of the nature of PTR through gA. In this paper we use the gramicidin A structure obtained by Townsley et al.³⁷ (PDB entry 1JNO). Our starting point in choosing an effective way to simulate this system is the empirical valence bond (EVB).³⁶ The main points of this

* Corresponding author. E-mail address: warshel@usc.edu.

method are described below for the case of n protonation sites (which are considered formally as bases) and one excess proton. In this case we describe the EVB quantum system in terms of diabatic states

$$\begin{aligned}\Psi_i &= B_1 B_2 \dots B_i H^+ \dots B_n \\ \Psi_j &= B_1 B_2 \dots B_j H^+ \dots B_n\end{aligned}\quad (1)$$

where $B_i H^+$ is the protonated form of the B_i protonation site (e.g., an H_3O^+).

Now, the i th diagonal element of the Hamiltonian of this system is described by a force-field like function that describes the bonding within donors, the bond of the proton to the i th base, as well as the nonbonded interactions in the system and its interactions with the surroundings (protein or water). More specifically, the diagonal elements are described by

$$\begin{aligned}H_{ii} = \epsilon_i &= \sum_m D[1 - \exp\{-\beta(b_m^{(i)} - b_{0,m}^{(i)})\}] + \\ &\sum_m (K_\theta/2)(\theta_m^{(i)} - \theta_{0,m}^{(i)})^2 + \sum_{k,k'} (Ar_{k,k'}^{-12} - Br_{k,k'}^{-6}) + \\ &\sum_{k,k'} 332 Q_k^{(i)} Q_{k'}^{(i)} (1 - \exp^{-\mu_s r_{k,k'}^2}) / r_{k,k'} - \sum_{k,k'} 166\alpha / r_{k,k'}^4 + \\ &\Delta^{(i)} + U_{Ss}^{(i)} + U_{ss} = \epsilon_i^0 + \Delta^{(i)} + U_{Ss}^{(i)} + U_{ss}\end{aligned}\quad (2)$$

where the $b^{(i)}$'s and $\theta^{(i)}$'s are respectively the bond lengths and bond angles in the quantum mechanical system composed of the n bases and the excess protons. $r_{k,k'}$ runs over all the nonbonded distances in the quantum system. The r^{-4} term represents an approximation for the inductive interaction between the solute charges. $U_{Ss}^{(i)}$ describes the interaction between the quantum system (the "solute") in its i th state and the surrounding classical system (the "solvent"), which includes water molecules and/or protein atoms. U_{ss} is the solvent-solvent classical potential surface. Finally, $\Delta^{(i)}$ is the so-called "gas-phase shift" that determines the relative energy of the diabatic states.³⁶ The off-diagonal elements (the H_{ij} 's) are described by empirical functions that are fitted to experimental information and ab initio calculation, and the ground-state energy, E_g , is obtained by diagonalizing the EVB Hamiltonian.

$$\mathbf{HC}_g = E_g \mathbf{C}_g\quad (3)$$

More detail on the nature of the EVB matrix elements for different systems is given elsewhere.^{23,36} In the present work we represent the cases where the bases are water molecules by a slightly modified version of the parameters used in ref 38. The EVB potential surface lends itself to convenient studies of the free energy profile for the PTR process. This is done by using a free energy perturbation/umbrella sampling (FEP/US) method that uses the percent of transfer between one EVB state to another as a mapping parameter, and then uses umbrella sampling to find the free energy of the ground-state surface along a special reaction coordinate defined by the energy gap between the EVB states.^{23,36} More specifically, the EVB approach changes the system adiabatically from one diabatic state to another. In the simple case of two diabatic states, this "mapping" potential, ϵ_m , can be written as a linear combination of the reactant and product potentials, ϵ_1 and ϵ_2 :

$$\epsilon_m = (1 - \theta_m)\epsilon_1 + \theta_m\epsilon_2 \quad (0 \leq \theta_m \leq 1)\quad (4)$$

When λ_m is changed from 0 to 1 in $n + 1$ fixed increments ($\theta_m = 0/n, 1/n, 2/n, \dots, n/n$), potentials with one or more of the

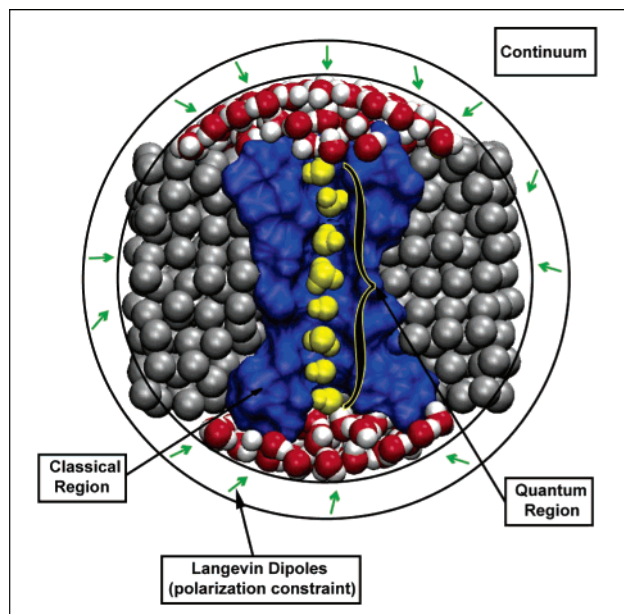


Figure 1. Showing the simulation system. The figure depicts the gA channel, the surrounding grid used to simulate the membrane region, the SCAAS water sphere, the chain of water molecules and the proton.

intermediate values of θ will force the system to fluctuate near the TS.

The free energy, ΔG_m , associated with changing θ from 0 to m/n is evaluated by the FEP procedure described elsewhere (see, e.g., chapter 3.3.2 in ref 36). The free energy functional that corresponds to the adiabatic ground-state surface, E_g (eq 3) is then obtained by the FEP-umbrella sampling (FEP/US) method,^{36,39} which can be written as

$$\Delta g(x') = \Delta G_m - \beta^{-1} \ln \langle \delta(x - x') \exp[-\beta(E_g(x) - \epsilon_m(x))] \rangle_m\quad (5)$$

where x is the generalized reaction coordinate, taken in the EVB approach as the energy gap between the reactant and product diabatic potentials ($x = \epsilon_j - \epsilon_i$). ϵ_m in eq 5 is the mapping potential that keeps x in the region of x' . If the changes in ϵ_m are sufficiently gradual, the free energy functional $\Delta g(x')$ obtained with several values of m overlap over a range of x' , and patching together the full set of $\Delta g(x')$ gives the complete free energy curve for the reaction. The FEP/US approach may also be used to obtain the free energy functional of the isolated diabatic states. For example, the diabatic free energy, Δg_1 , of the reactant state can be calculated as

$$\Delta g_1(x') = \Delta G_m - \beta^{-1} \ln \langle \delta(x - x') \exp[-\beta(\epsilon_1(x) - \epsilon_m(x))] \rangle_m\quad (6)$$

The diabatic free energy profiles of the reactant and product states represent microscopic equivalents of the Marcus' parabolas.^{40,41} The reorganization energy, λ_{ij} , of the $i \rightarrow j$ reaction step can be obtained directly from the plots of the diabatic curves (as in Figure 3) or by using

$$\lambda_{i \rightarrow j} = 1/2(\langle \epsilon_j - \epsilon_i \rangle_i - \langle \epsilon_j - \epsilon_i \rangle_j)\quad (7)$$

The use of the energy gap as a reaction coordinate appears to provide a very powerful tool for studies of PTR because the electrostatic contribution to the energy gap corresponds to the generalized solvent coordinate, which is hard to explore by other approaches. The EVB approach also provides convenient

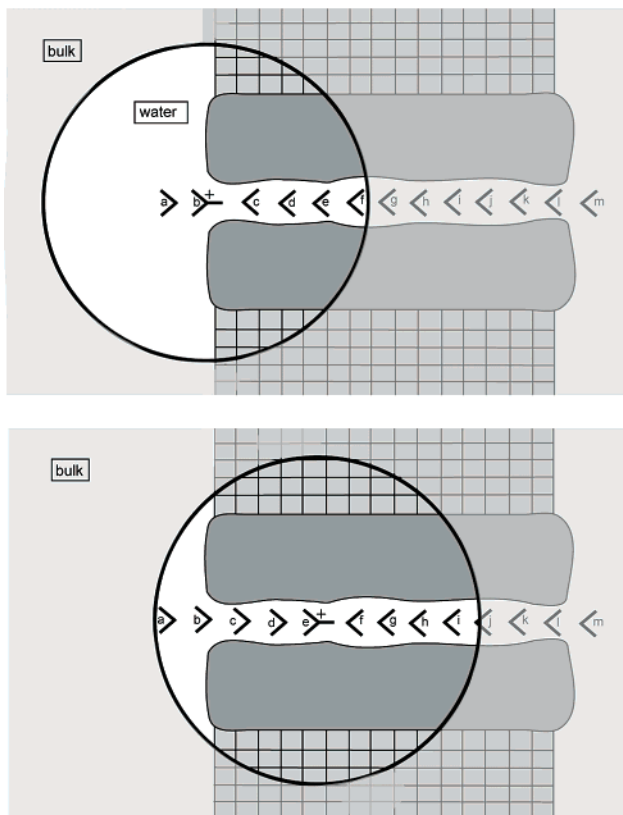


Figure 2. Schematic representation of the simulation procedure. As illustrated in the figure, we move the center of the SCAAS water sphere with the transferred charge. This and the corresponding bulk correction allow us to obtain stable electrostatic energies. Note that the SCAAS and LRF treatment treats the regions inside the sphere by a fully microscopic approach (see Figure 1) that takes, of course, the channel flexibility into account. The figure also depicts the notation for the EVB water molecules.

analytical first derivatives that make it easy to explore the actual dynamics of the PTR process (being limited, however, by the available computer time).

With the EVB surface we can study, in principle, any PTR process. However, this requires extremely long computer times if one is interested in processes in the range of microseconds or longer. Thus, it is important to simplify the simulation system and to convert the EVB surface that treats explicitly the entire protein to a simpler effective potential that treats explicitly only the molecules that are involved directly in the PTR (referred to here as the active space). This can be done by moving to a simpler effective EVB surface using the same type of solute surface as in eq 2, while omitting the explicit solute–solvent and solvent–solvent terms (the U_{ss} and U_{ss} terms) and replacing them by implicit terms using

$$\bar{\epsilon}_i = \epsilon_i^0 + \bar{\Delta}_i + (\hbar\omega_Q/2)[(Q_{i,k(i)} + \delta)^2 + (Q_{i,k'(i)} - \delta)^2] \quad (8)$$

$$\bar{E}_{\text{tot}} = \bar{E}_g + \sum_i (\hbar\omega_Q/2)[(Q_{i,k(i)}^2 + B(Q_{i,k(i)} - Q_{i,k'(i)})^2)] \quad (9)$$

where the Q 's are the solvent coordinates that are given by the electrostatic component of the energy gap $(-\hbar\omega_Q\delta)Q_{ij} = \epsilon_j^{\text{el}} - \epsilon_i^{\text{el}}$, δ is the dimensionless origin shift of the solvent coordinate, ω_Q is the effective vibration of the solvent, \bar{E}_g is the lowest eigenvalue of eq 3, and the B term represents the coupling between the solvent coordinates. Equation 4 is written for the case of a chain of water molecules, so that we assign a

solvent coordinate to each pair of oxygens. In this case, the index i corresponds to a proton on the i th oxygen inside the chain, and $k(i)$ and $k'(i)$ correspond to the oxygens before and after i , respectively. When i is the first oxygen, there is no $Q_{i,k'}$. Now, using eq 9 we obtain

$$\bar{E}_{\text{tot}} = \mathbf{C}_g^T \bar{\mathbf{H}}^0 \mathbf{C}_g + \sum_i (\hbar\omega_Q/2)[(C_g^i)^2((Q_{i,k(i)} + \delta)^2 + (Q_{i,k'(i)} - \delta)^2) + \sum_i (Q_{i,k(i)}^2 + B(Q_{i,k(i)} - Q_{i,k'(i)})^2)] \quad (10)$$

where $\bar{\mathbf{H}}^0$ is the solute Hamiltonian and \mathbf{C}_g is the ground-state eigenvector of the simplified EVB Hamiltonian with the diagonal elements of eq 8. The free energy, \bar{g} , associated with the energy surface, \bar{E}_g (here the free energy accounts for the average over the coordinates of the active space), is treated as the effective free energy surface that includes implicitly the rest of the system. That is, we use

$$g(\mathbf{r})_{\text{eff}} = \bar{g}_g(\mathbf{r}) \quad (11)$$

where \mathbf{r} are the coordinates of the active space. In doing so, we note that in this simplified expression we treat the environment implicitly by adjusting the $\bar{\Delta}^{(i)}$ while imposing the requirement

$$\begin{aligned} (\Delta G_{i \rightarrow j})_{\text{eff}} &= (\Delta G_{i \rightarrow j})_{\text{complete}} \\ (\Delta g_{i \rightarrow j}^\ddagger)_{\text{eff}} &= (\Delta g_{i \rightarrow j}^\ddagger)_{\text{complete}} \end{aligned} \quad (12)$$

where $(\)_{\text{eff}}$ represents the quantity obtained with the effective EVB potential and $(\)_{\text{complete}}$ designates the results obtained when the EVB of the entire system is included explicitly. For convenience we usually determine $(\Delta G_{i \rightarrow j})_{\text{complete}}$ (and the corresponding $\Delta^{(i)}$ values of the effective model) by the semimacroscopic electrostatic calculations outlined below.

With the effective potential defined above, it is possible to examine the time dependence of PTR processes by Langevin dynamics (LD) simulations. That is, the time dependence of the system is determined by a Langevin equation:⁴²

$$m_i^* \ddot{r}_{i\alpha} = -m_i^* \gamma_i \dot{r}_{i\alpha} - \partial \Delta g_{\text{eff}} / \partial r_{i\alpha} + A_{i\alpha}(t) \quad (13)$$

where Δg is the effective potential of eq 11, i runs over the ions, α runs over the x , y , and z Cartesian coordinates of each ion, m_i^* is the effective mass of the i th particle, γ_i is the friction coefficient for the i th ion, and $A_{i\alpha}$ is a random force, which is related to γ_i through the fluctuation–dissipation theorem.⁴³

The corresponding LD equation for the solvent coordinate is now expressed as

$$m_Q \ddot{Q}' - m_Q \gamma_Q \dot{Q}' - \partial \bar{E}_{\text{tot}} / \partial Q_i + A_i(t) \quad (14)$$

where $Q = (m_Q \omega_Q / \hbar)^{1/2} Q'$, $\delta = (m_Q \omega_Q / \hbar)^{1/2} \delta'$, and γ_Q and m_Q are the effective friction and effective mass of the solvent.⁴⁴

The above approach for calculations of the effective free energy can be approximated by using the modified Marcus' relationship^{23,36,45}

$$\Delta g_{i \rightarrow j}^\ddagger = (\Delta G_{i \rightarrow j}^0 + \lambda)^2 / 4\lambda - \bar{H}_{ij}(x^\ddagger) + \bar{H}_{ij}^2(x_0^{(i)}) / (\Delta G_{i \rightarrow j}^0 + \lambda) \quad (15)$$

where $\Delta G_{i \rightarrow j}^0$ is the free energy of the reaction, and H_{ij} is the off-diagonal term that mixes the two relevant states (the average value at the transition state, x^\ddagger , and at the reactant state, $x_0^{(i)}$, are designated by the corresponding \bar{H}). The first term in this expression is the regular Marcus' equation,⁴⁰ which corresponds

to the intersection of Δg_1 and Δg_2 at x^\ddagger . The second and third terms represent, respectively, the effect of H_{12} at x^\ddagger and $x_0^{(i)}$.

The EVB simulation system is described in Figure 1. It consists of the gA channel (constructed from PDB 1JNO), an excess proton, a chain of 15 water molecules that constitute the EVB quantum region, and a membrane (modeled by a grid of nonpolar atoms) that surrounds the channel in its x and y directions. This system is truncated to a radius R (typically 24 Å) and surrounded by a water sphere subjected to the surface constraint all atom solvent (SCAAS) boundary conditions (see refs 46 and 47) and treated by the local reaction field (LRF) long-range treatment.⁴⁸ The membrane grid has a spacing of 2.5 Å (grid size is $30 \times 30 \times 20$ Å), and each membrane atom is represented by an induced dipole with a polarizability of ~ 1 Å³. The center of the SCAAS sphere is taken as the midpoint between site α and β when modeling PT between these sites. The corresponding simulation boundaries are described schematically in Figure 2. The effect of having a spherical rather than correct geometry was then estimated macroscopically using the relationship⁴⁹

$$\Delta\Delta G_{\text{sol}} \approx 83[1/\bar{a} - 1/L] \quad (16)$$

where the energies and distances are given in kcal/mol and Å, respectively. Equation 16 has been derived for the case where the simulation sphere of a radius \bar{a} is in the center of a membrane of length L when $\bar{a} < L$ and interpolating the correction to zero when the center approaches the membrane boundaries. The resulting correction of about 2 kcal/mol is an upper limit for our case, where $\bar{a} \approx 24$ Å. The above approach gave more stable and reliable results than those obtained using nonspherical boundaries (see ref 50 for a related treatment of charge transfer in a membrane protein). The simulation system was treated by the standard simulation protocol of the MOLARIS simulation program,^{47,51} where the EVB mapping of each PT step involved 30 θ_m values with a 10 ps simulation time for every step. The simulations were done at 300 K with time steps of 1 fs.

The EVB QM system includes 15 water molecules and a proton. The two end water molecules only serve to provide proper boundaries and are not protonated in any EVB state. This leads to a 13 state EVB Hamiltonian. These states are designated here as a, b, \dots, l, m , where state j has the proton attached to the j th water molecule.

In constructing the simulation system for the simplified EVB calculations, we kept the water molecules of the "active space" near their average positions in the full model by using a Cartesian position restraint ($V''_{\text{rest}} = 1/2K(\mathbf{r}_i - \mathbf{r}_i^0)^2$) with $K = 10$ kcal·mol⁻¹·Å⁻². We also added a distance restraint of the form $V''_{\text{rest}} = 1/2K(b_{ij} - b_{ij}^0)^2$ with $K = 4$ kcal·mol⁻¹·Å⁻² between the oxygens of nearby water molecules. The LD simulations were done with the MOLARIS simulation program, considering the given chain of donor and acceptors. The optimal time steps for the underdamped LD simulations (eqs 13 and 14) were 1 fs. The reduced masses and friction coefficients were the same as those used in ref 44. It is important to note that ref 44 also discusses in length the evaluation of the dynamical parameters and demonstrates that we obtain similar dynamics in the full EVB and the simplified EVB models. The Hamiltonian parameters for both the simplified and full EVB simulations were those used in ref 44. The validity of these parameters is also demonstrated in this work, where we compare the reorganization energies obtained by both models.

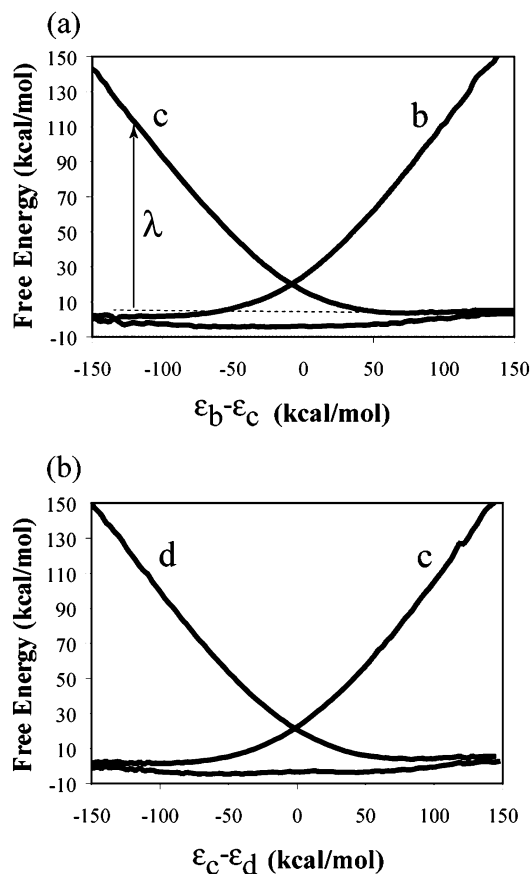


Figure 3. Diabatic (intersecting curves) and adiabatic (flat curve) free energy diagrams, obtained by the full EVB treatment, for two representative PT steps: (a) shows $b \rightarrow c$; (b) shows $c \rightarrow d$. The figure also relates the reorganization energy to the diabatic curves.

TABLE 1: Calculated Charging Free Energies for the $\text{H}_2\text{O} \rightarrow \text{H}_3\text{O}^+$ Process for Different Sites in the GA Channel^a

| site | $\langle \Delta G_{\text{sol}}^{(i)} \rangle$ |
|------|---|
| bulk | -99.8 |
| a | -97.1 |
| b | -99.2 |
| c | -97.6 |
| d | -95.0 |
| e | -93.2 |
| f | -94.1 |
| g | -92.7 |
| h | -94.1 |

^a The calculations of the charging free energies (the ΔG_{sol}) were done by the FEP approach described in the text. The reported values (in kcal/mol) correspond to an average over calculations with six different initial conditions. The results from h to m are taken to be equal to those in f to a, due to the symmetry of the system.

III. Results

At the first step of our study we performed EVB-FEP/US calculations of the free energy function for a stepwise PTR in gA. Typical results for two steps are given in Figure 3, and the use of these step-by-step mappings in constructing the overall profile is described below. We also used FEP adiabatic charging procedures (e.g., Warshel et al.⁵²) to evaluate the free energy of the $\text{H}_2\text{O} \rightarrow \text{H}_3\text{O}^+$ process, which should tell us about the electrostatic free energy of each adiabatic state relative to the corresponding free energy in water. The corresponding FEP results were obtained by mutating a water molecule with one extra nonpolar atom to H_3O^+ , in the given site, and subtracting from the resultant free energy the corresponding gas-phase free energy. The calculated FEP results are summarized in Table 1.

The calculations appear to give quite stable results with a relative error of about 1.5 kcal/mol, as was judged by repeating the calculations with different initial configurations. Much larger errors and larger size dependence were obtained when we did not use the LRF long-range treatment, or when we did not follow the SCAAS procedure. Now the EVB-FEP/US calculations gave a somewhat larger error (about 3 kcal/mol) due to the steep dependence of the intramolecular terms (the electrostatic contributions appeared to be very stable). In view of this problem, we adjusted the gas-phase shifts (the $\Delta^{(i)}$ values of eq 2) so that the ΔG_{ij} obtained by the EVB-FEP/US will coincide with the corresponding values obtained by the FEP charging calculations. In this way we adopted a philosophy where the shape of the surface is determined by the EVB mapping, but the energy of each step is determined by a FEP approach. It seems to us that this may provide, at present, the most reliable option in heterogeneous environments where the electrostatic calculations are challenging. We would like to point out, however, that the present EVB mapping results are very encouraging (despite the 3 kcal/mol error range) in view of the major difficulties encountered in our PMF studies of ion transport, which involves the z coordinate as a mapping parameter (see discussion in ref 53 and also in refs 54 and 55). The difference is that in the case of PT reactions or other charge transfer processes, the EVB mapping uses a physically correct solvent coordinate and thus provides a much better sampling than that obtained by using the ion position as the mapping parameter. Of course, it would be useful to couple the solvent coordinate to the mapping of the solute position in studies of ion transport (rather than PT) processes, and this is currently under progress in our lab.

The EVB approach allowed us to examine the nature of the solvent reorganization effect by considering the diabatic free energy functions of eq 6. As seen from Figure 3, the calculated reorganization energy in each PT step is quite significant. A large part of the reorganization energy is due to the solute coordinate itself, and this part is somewhat arbitrary, because we can reduce both H_{ij} and the solute reorganization energy while retaining the same ground state surface. However, the “outer sphere” reorganization (Figures 3 and 4) is also quite significant, this contribution reflects the reorganization of the channel dipoles and the reorganization of the water molecules around the donor and acceptor. Interestingly, the effect of the contribution of the channel reorganization is as large as that of the water file (see Table 2). This point is important in view of studies that focus only on the reorientation of the water file and consider this effect to represent the main solvent coordinate. It is also useful to consider the EVB free energy surface in terms of its solute and solvent coordinates. This is done in Figure 5 for a typical PT step, where it appears that the solvent coordinate plays a major role in controlling the PT process. This effect is retained in our simplified model.

To establish the similarity of the simplified and the full EVB treatments, we compare in Figure 6 the corresponding surfaces. As seen from the figure, the surfaces for the stepwise PT are quite similar. Because both the simplified and the full EVB models have similar treatment of the mixing between the different states, they should also provide a similar trend for concerted PTR processes.

It is also important to compare the dynamics of the full model and the simplified model. This is done in Figure 7, where we compare the autocorrelation of the time dependent energy gap ($\epsilon_j - \epsilon_i$) for a trajectory that is forced to stay on ϵ by using the ϵ_m of eq 4. For a formal discussion, see ref 56. The figure

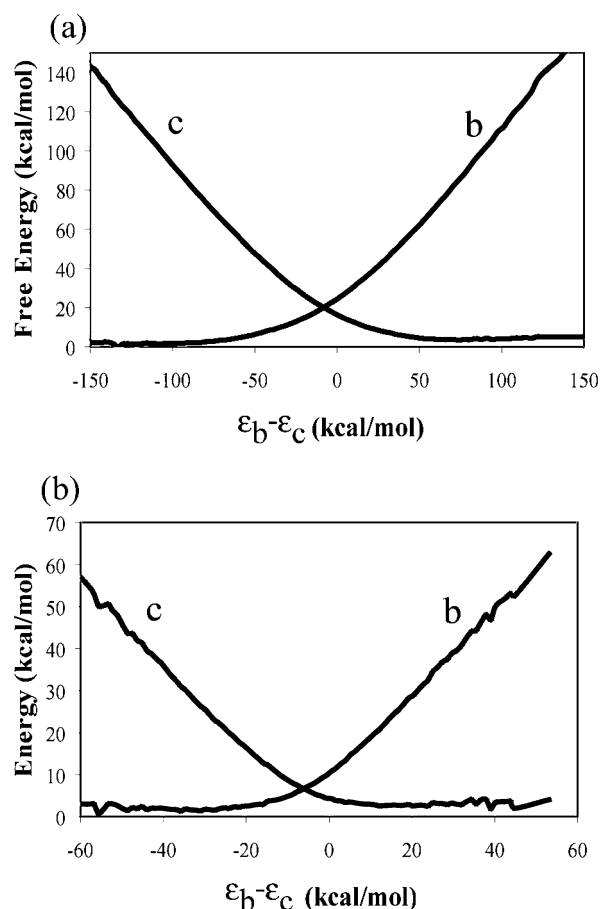


Figure 4. Analysis of the contribution to the reorganization energy from the solute, the protein, and the water file (the calculations are done for the $c \rightarrow b$ transfer). The reorganization energy can be obtained approximately by multiplying by four the energy of intersection of the diabatic state (the intrinsic barrier). (a) shows the total reorganization energy; (b) shows the electrostatic reorganization energy.

TABLE 2: Contributions to the Outer Shell Reorganization Energy from the Channel Dipoles and the Water Dipoles^a

| step | λ_{qu} | λ_{qw} |
|-------------------|----------------|----------------|
| bulk | 0 | 30 |
| $c \rightarrow d$ | 34 | 2 |
| $d \rightarrow e$ | 29 | 1 |

^a The reorganization energy contribution (in kcal/mol) of the channel dipoles (λ_{qu}) and of the water molecules (λ_{qw}) are given in kcal/mol. These contributions were evaluated using eq 7.

indicates that the simplified model captures the dynamics of the full model. Here we note that the similarity of the autocorrelation function is encouraging, considering the fact that the simplified and full models are quite different.

Considering the stability of our FEP/US calculations of the stepwise PT processes, we used the calculations to construct the overall surface for a stepwise PTR (the effect of concerted motion will also be discussed). The resultant piecewise mapping is shown in Figure 8. As seen from the figure, the PTR adiabatic profile is quite flat, reflecting the effect of the off-diagonal coupling. Now, despite the flatness of the profile along the channel, the highest points in the profile are raised by about 5–6 kcal/mol relative to the corresponding energy in water. This reflects the loss of solvation moving from the bulk solvent to the center of the channel. This effect is similar to the corresponding effect in the profile for ion transport,⁵⁷ except that the effect of H_{ij} reduces the barrier between adjacent sites.

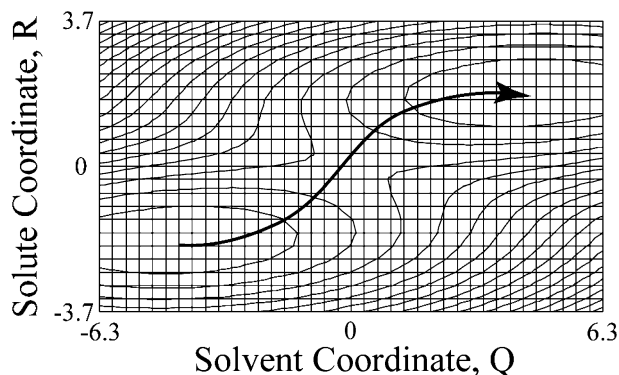


Figure 5. Illustrating the nature of the free energy landscape for the $b \rightarrow c$ step in the solute–solvent coordinate space.

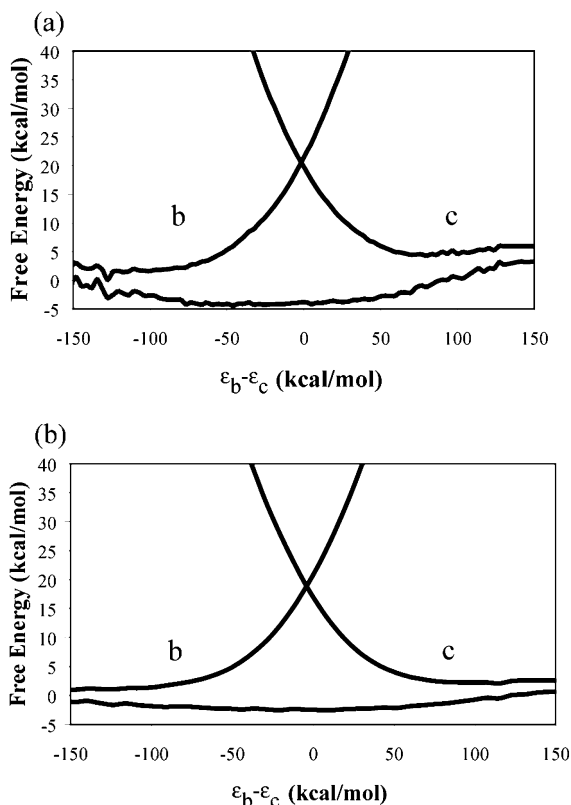


Figure 6. Comparing the EVB profile for the full (a) and simplified (b) models for the $b \rightarrow c$ step. The figure demonstrates that both models give similar reorganization energies.

It is interesting to note that the calculated activation free energy for the stepwise adiabatic transfer is about 5 kcal/mol when measured, respectively, relative to the minimum at the entrance to the channel. This seems reasonable, as can be judged from the effective activation free energy of about 6.4 and 4.8 kcal/mol measured in glycerylmonooleatedecane (GMO) and in a phospholipid membrane, respectively, by Chernyshev and Cukierman.⁵⁸ However, because it is hard to assess the relationship between the calculated barrier and the observed properties of the channel without simulating the relevant proton current, we will try to obtain a more direct estimate. Interestingly, the barrier relative to the bulk is about 6 kcal/mol, but we are not sure if this is significant in view of the estimated error range (~ 1 – 2 kcal/mol).

With a calculated free energy profile (whose stepwise section is shown in Figure 8), our next task is to examine the time dependence of the PTR process. The first option is to use direct MD simulations with the full EVB model. This approach is,

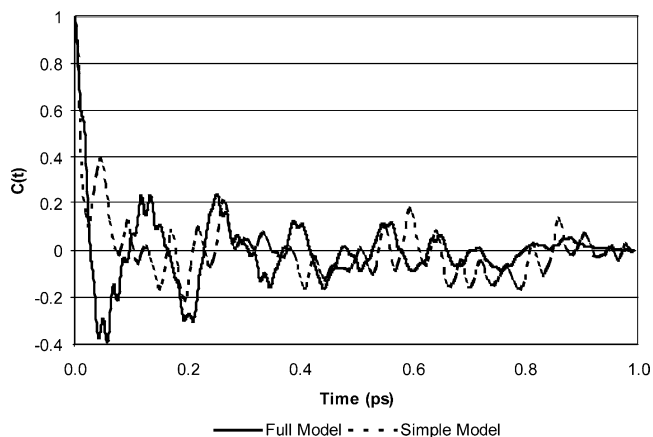


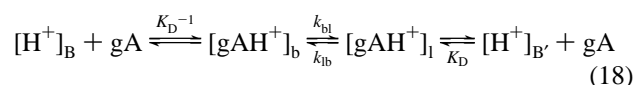
Figure 7. Autocorrelation of the energy gap for the full (black line) and simplified (dashed line) model.

however, impractical when the barrier is higher than a few kcal/mol. Thus, we examined the PTR process by the simplified EVB model and the result of a typical LD trajectory is presented in Figure 9. The calculated average transfer time was found to be about 4×10^{-8} s. To relate this finding to the experimental finding, it is useful to examine the transfer time and the corresponding current under the influence of an external potential. This is done by adding the effect of the external potential to the $\bar{\Delta}_i$ of eq 8. This is done by using

$$\Delta_i(Z_i) = -V(Z_i/L) + \Delta_i(V=0) \quad (17)$$

where Z_i is the position of the proton on the i th site and L is the length of the membrane. The same approach has been basically used in our previous work⁵⁹ and in earlier works of Chang and co-workers.⁶⁰ Using the above approach, we obtained a transfer time of ~ 20 ns and ~ 40 ns for $V = 200$ mV and 100 mV, respectively, corresponding to a single ion current of 4.0 and 2.0 pA at these potentials (see below).

To obtain a qualitative estimate of the corresponding observed value, we represented the conductance process at low $[H^+]$ by Michaelis–Menton type kinetics, writing



where B and B' designate the bulk at both sides of the membrane, and $[gAH^+]_b$ designates the concentration of $[H^+]$ at site a . Now at the limit of low $[H^+]$ and assumed quasi-equilibrium, we can write for the forward current, I^+ , associated with the $b \rightarrow l$ transfer, the expression

$$I^+ \cong (e^-)k_{bl}[gAH^+]_a \cong (e^-)k_{bl}[H^+]_B[gA]/K_D \quad (19)$$

where e^- is the electron charge and k_{bl} and K_D are defined in eq 18. Estimating K_D from reference 61 as 10 mM, we obtain for $[H^+] = 5$ mM,

$$I^+ = (e^-/\tau_{bl})0.5 \quad (20)$$

where τ_{bl} is the average time of transfer from b to l . Now with the experimental estimate of a current between 1 pA to 0.5 pA at 5 mM $[H^+]$ and 100 mV and with the approximation of $I^+ \cong I$ for sufficiently large potentials we obtain

$$I_{(pA)} = (1.6 \times 10^5) \times 0.5/\tau_{bl}(\text{ps}) \approx 0.5 \text{ pA} \quad (21)$$

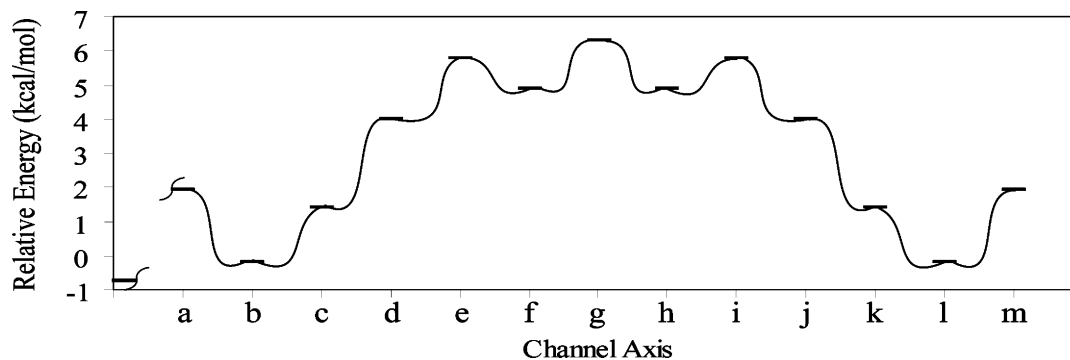


Figure 8. Overall free energy profile for stepwise PTR. The relative energy of the bulk is designated to the left of point a.

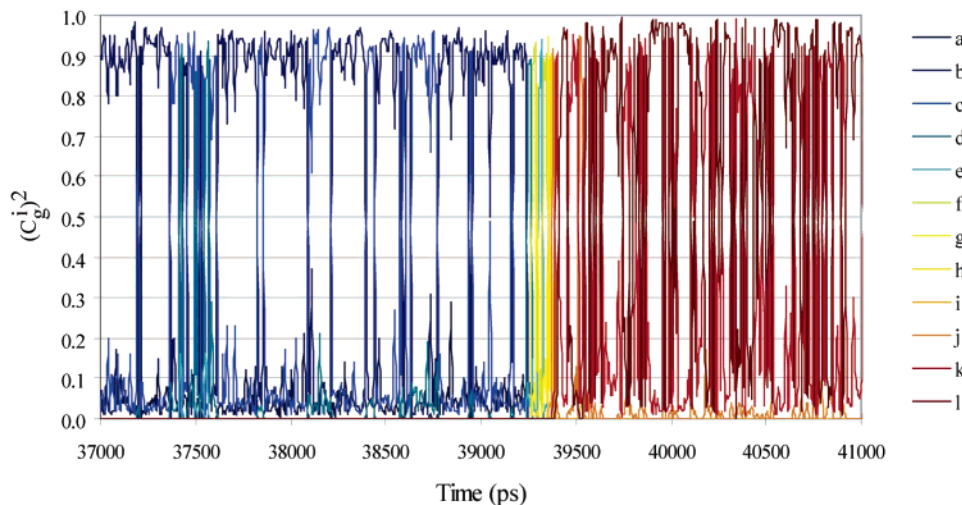


Figure 9. Showing a typical LD trajectory for a PTR across the gA channel under the influence of a 100 mV potential. The figure describes the probability amplitudes of being in the different EVB states (the $(C_i^g)^2$) as a function of time. The colors that correspond to each state are indicated on the right side of the figure. The trajectory stays at the a–c region until about 39 ps, so that we only depict the time dependence of the system after 37 ps.

where, as indicated, I and τ are given in picoamperes and picoseconds, respectively. This gives an upper limit of $\tau_{bl} = 1.6 \times 10^5 \text{ ps} = 160 \text{ ns}$. Of course, it would be useful to perform a more detailed current voltage analysis, and this will be done in the future. However, our main point is the establishment of the fact that the calculated transfer time of $\sim 40 \text{ ns}$ is consistent with the experimental studies of PTR in gA.

To gain more confidence about the validity of the simplified EVB model, we studied the time dependence of past processes where both the full and the simplified models can be used. In particular, we examined the transfer from site d to site b in both models, and the corresponding results are depicted in Figure 10. As seen from the figure, both models give a similar dynamical description. This finding, and the additional analysis provided in ref 44 indicates that the simplified EVB model can be used with confidence to explore the PTR in gA.

IV. Concluding Remarks

This work examined the molecular basis of proton conductance through the gA channel by using a full EVB model to obtain the free energy profile and then using a simplified EVB model to obtain the time dependence of the PTR process. It was found that the barrier associated with the electrostatic energy of the transferred proton determines the rate of the PTR process. This indicates that once the electrostatic barrier is significant, the PTR process is controlled by this barrier rather than by the water orientational effects of the Grotthuss mechanism.

Previous studies of the dynamics of PTR in the gA channel have followed the picture of Nagle and co-workers^{14,15} and separate the PTR process to a step that involves the reorientation of the water file in the absence of the proton (the “Turn” step) and a transfer of the proton along the perfectly oriented file (the “Hop” step). For example, this seems to be the case in studies of PTR in nonpolar channels that were thought to be relevant to the gA system.¹⁷ Such studies led to the assumption that the water reorientation step is rate limiting and that the Hop step is very fast. Although some elements of the previous studies are instructive, we believe that the overall conclusion is problematic. First, the assumption that the orientation of the unprotonated water file is rate limiting does not reflect the proper solvent reaction coordinate. This can be seen, for example, in the case of a very long channel where it is obvious that the very large energy of rotating the long water file is not related to the proper reorganization energy, which usually reflects the polarization of the channel and water dipoles around the pair of water molecules involved in each transfer step. This point is particularly crucial when the electrostatic energy of the transferred proton increases along the PTR path. Here the use of the EVB method allows us to explore in a consistent way the effect of the polar fluctuations and the role of the overall electrostatic energy of the transferred proton. Second, the finding that the actual proton transfer is not rate limiting, and the free energy profile for transferring the proton along the oriented water file has a minimum at the center of the channel, seems to be inconsistent with the expected stabilization of the proton in the

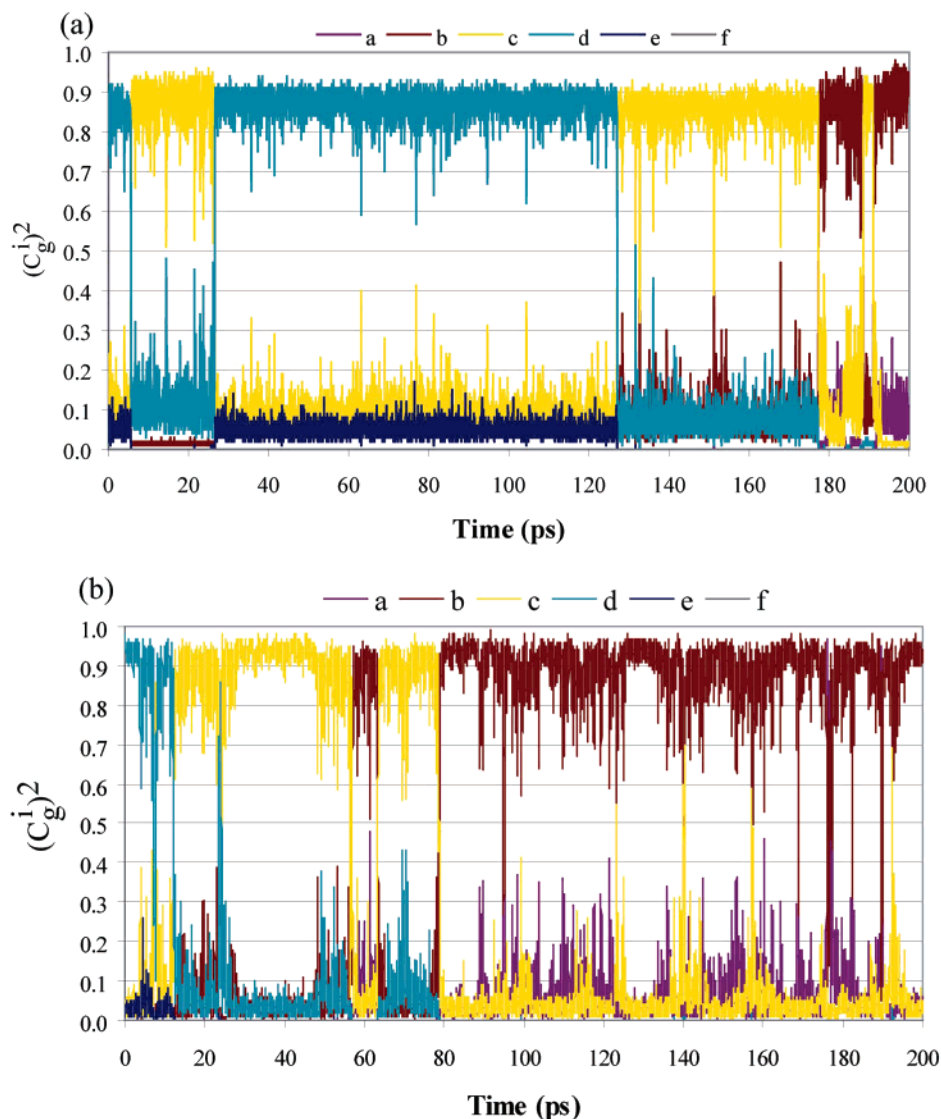


Figure 10. Comparing the time dependence of the full and simplified model for a PTR from d to b in gA in the (a) full and (b) simplified models. Notation as in Figure 9. Although the detailed dynamical behavior is not identical, the approximate transfer time is similar.

bulk water. Further discussion of this important issue is given in ref 44 where we consider the validity of different studies that overlooked the importance of the electrostatic barrier.

It is useful to realize that the charging free energies obtained by the FEP approach reflect the reorganization and rearrangement of the water file and the channel that leads to configurations that give the lowest potential energies for the given position of the proton (these potential energies give the largest contributions to the corresponding free energy). Thus, the EVB mapping that moves the proton from site *i* to site *j* does lead the proton along the least energy path for diabatic transfer. Of course, one has to take into account the delocalization effects, but this is accomplished quite effectively by the EVB mixing procedure.

It is also important to clarify a point that is frequently misunderstood. That is, our EVB approach uses as zero order diabatic states the localized H_3O^+ states and then mixes them to obtain the proton delocalization. This procedure adds the solvation of the localized H_3O^+ states by the environment (in its given polarization) to the diagonal EVB Hamiltonian. Now this approach is much more consistent than the option of solvating the mixed states (e.g., H_5O_2^+ states) because solvating adiabatic states is equivalent to solvating gas-phase QM systems in an uncoupled QM/MM treatment that has been shown to be

very problematic^{62,63} (see also a discussion in ref 44 of a related problem in the so-called MS-EVB approach,^{64,65} which is otherwise very similar to our EVB treatment). Now, in the EVB treatment we do obtain, of course, delocalized H_5O_2^+ and other delocalized states in solutions and proteins, but this is obtained after we diagonalize the solvated EVB Hamiltonian. Here it is useful to realize that the diabatic basis functions are just mathematical constructs rather than a physical reality. Only the adiabatic ground state represents a physical reality (it is the actual observable). Thus, although the EVB considers the solvation of the H_3O^+ states, it reproduces the correct and consistent amount of delocalization when this exists. To illustrate this point, we show in Figure 11 the charge distribution of the water file during the transfer process. Clearly we have a delocalized proton as explained above. However, the correct profile that generates this charge distribution is obtained from the ground state that mixes the localized H_3O^+ diabatic states.

Our EVB mapping procedure indicated clearly that the free energy profile for a stepwise transfer is strongly affected by the electrostatic effect of the channel, and that such a profile involves sections where the proton is less stable than in the bulk solvent. Now, as demonstrated in our recent works,^{44,66} the adiabatic PTR does follow the diabatic profile, especially

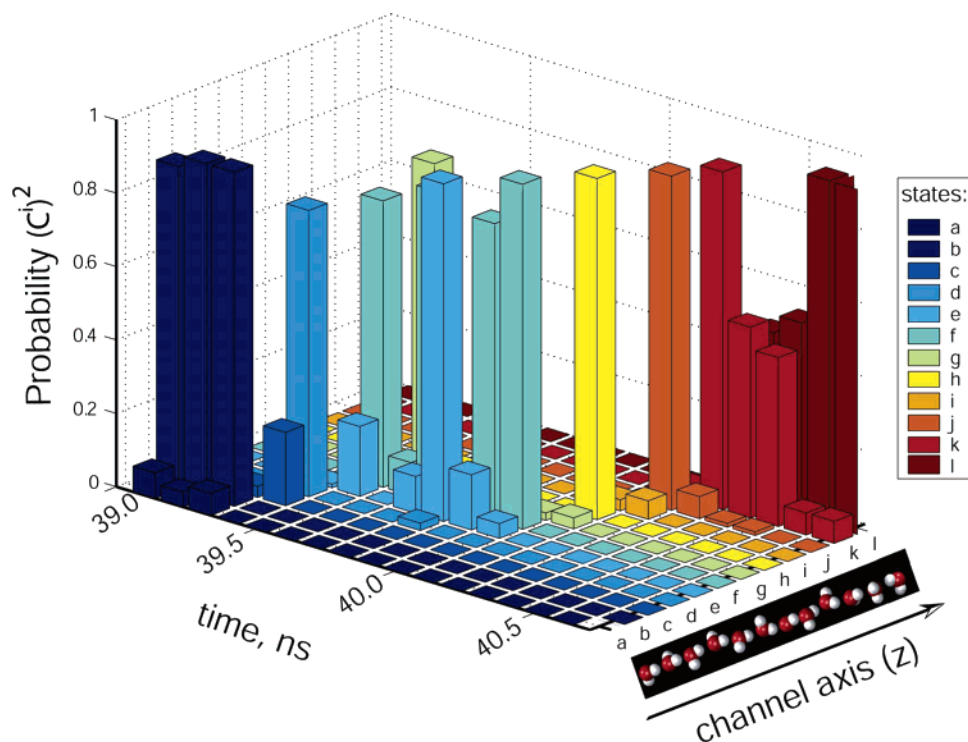


Figure 11. Illustrating the delocalized nature of the transferred proton. The figure focuses on the time when a productive trajectory transfers the system from a to l and displays the $(C_g^i)^2$ for the different sites as a function of time.

when the profile has a significant barrier and when the barrier involves more than two sites. When the barrier involves a single site, the proton can move in a concerted way, and thus has a lower barrier (see discussion in ref 44). Now, as seen from Figure 9, we have some cases with a single site barrier (e.g., $d \rightarrow e \rightarrow f$) so that the $d \rightarrow f$ barrier can be lower than $\Delta G_{d \rightarrow e}$ due to a concerted motion, but it cannot be lower than $\Delta G_{d \rightarrow f}$. Thus, even with the possibility of a concerted effect (which is fully captured by the simplified model) the overall barrier is determined by $\Delta G_{b \rightarrow h}$, which is not negligible. With this in mind, we conclude that the PTR in gA is indeed determined by the diabatic electrostatic barrier, reflecting, of course, the adiabatic mixing effects (see below).

The careful considerations of the present study help to account for the difference between H^+ and Na^+ transfer. Here we have to consider two effects. First, we have the obvious effect of the EVB off-diagonal mixing term. This term flattens the diabatic barrier of the PT process and thus smooths down the electrostatic barrier so that $\Delta G_{i \rightarrow j}^+ \cong \Delta G_{i \rightarrow j}$. This gives a lower profile than that obtained for transport of an ion of a similar size. Second, single site barriers such as the $d \rightarrow f$ transfer can be reduced. Thus, the overall barrier for the PTR process is smaller than that for Na^+ . Now in the limit of zero solvation barrier, the effect of the off-diagonal term will lead to a barrierless PTR, but in gA and other channels the energy price of moving the charge from water to the channel is the key factor. With this view in mind, we conclude that PTR and ion transfer share usually a common rate determining factor, namely, the electrostatic barrier.

The present conclusions depend of course on the validity of our FEP profile for the H_3O^+ ion. Here we would like to point out that our study reflects the state of the art free energy calculations with optimal boundary conditions and long-range treatment. Furthermore, despite concerns expressed about the ability of current simulation approaches to produce reliable profiles for ion transport in gA,^{54,55} we find that at least with

the EVB treatment, we obtain very stable results (which is much more stable than the results we obtained before for Na^+ or K^+). These results are not drastically sensitive to the van der Waals' parameters, because small changes in these parameters lead to similar changes in the solvation of the ion in the protein and in solution. We also would like to clarify that our FEP calculations capture the full flexibility of the channel, and the effect of the membrane induced dipoles. Finally, our current simulations are not drastically dependent on the friction constant used (decreasing γ by a factor of 2 increases the current by a factor of 2).

In judging the general validity of our proposals, that the electrostatic energy of the proton rather than the orientation of the unprotonated water determines PTR rates, it may be instructive to think about the observed current/voltage relationship.⁵⁸ That is, the observed linear relationship seems to be more consistent with the effect of the external field on the proton charge than any alternative model, such as the effect of the external field on the dipole moment of the neutral file. More systematic studies of this issue will clearly be useful.

In summary, the present work established that PTR processes are still controlled by the electrostatic barrier, even in channels with a relatively low electrostatic barrier. Of course, in the case of no electrostatic barrier (e.g., PTR in water) the Grothuss orientational effect is the rate-limiting factor.

Acknowledgment. This work was supported by NIH grant 40283. We are grateful to Mats H. M. Olsson for useful discussions and kind help.

Supporting Information Available: An instructive animation of a proton-transfer process in avi format. This material is available free of charge via the Internet at <http://pubs.acs.org>.

References and Notes

- (1) Warshel, A. *Proc. Natl. Acad. Sci. U.S.A.* **1984**, *81*, 444.
- (2) Mitchel, P. *Nature* **1961**, *191*, 144.

- (3) Ermler, U.; Fritzsche, G.; Buchanan, S. K.; Michel, H. *Structure* **1994**, *2*, 925.
- (4) Okamura, M. Y.; Feher, G. *Annu. Rev. Biochem.* **1992**, *61*, 861.
- (5) Gennis, R. B. *Biomembranes: Molecular Structure and Function*; Springer-Verlag: New York, 1989.
- (6) Wikstrom, M. *Curr. Opin. Struct. Biol.* **1998**, *8*, 480.
- (7) Girvin, M. E.; Rastogi, V. K.; Abildgaard, F.; Markley, J. L.; Fillingame, R. H. *Biochemistry* **1998**, *37*, 8817.
- (8) Luecke, H.; Schobert, B.; Richter, H. T.; Cartailler, J. P.; Lanyi, J. K. *J. Mol. Biol.* **1999**, *291*, 899.
- (9) Sass, H. J.; Buldt, G.; Gessenich, R.; Hehn, D.; Neff, D.; Schlesinger, R.; Berendzen, J.; Ormos, P. *Nature* **2000**, *406*, 649.
- (10) Royant, A.; Edman, K.; Ursby, T.; Pebay-Peyroula, E.; Landau, E. M.; Neutze, R. *Nature* **2000**, *406*, 645.
- (11) Luecke, H. *Biochim. Biophys. Acta* **2000**, *1460*, 133.
- (12) Ostermeier, C.; Harrenga, A.; Ermler, U.; Michel, H. *Proc. Natl. Acad. Sci. U.S.A.* **1997**, *94*, 10547.
- (13) Yoshikawa, S.; Shinzawa-Itoh, K.; Nakashima, R.; Yaono, R.; Yamashita, E.; Inoue, N.; Yao, M.; Fei, M. J.; Libeu, C. P.; Mizushima, T.; Yamaguchi, H.; Tomizaki, T.; Tsukihara, T. *Science* **1998**, *280*, 1723.
- (14) Nagle, J. F.; Morowitz, H. J. *Proc. Natl. Acad. Sci. U.S.A.* **1978**, *75*, 298.
- (15) Nagle, J. F.; Mille, M. *J. Chem. Phys.* **1981**, *74*, 1367.
- (16) Marrink, S. J.; Jahnig, F.; Berendsen, H. J. *Biophys. J.* **1996**, *71*, 632.
- (17) Pomes, R.; Roux, B. *Biophys. J.* **1998**, *75*, 33.
- (18) Brewer, M. L.; Schmitt, U. W.; Voth, G. A. *Biophys. J.* **2001**, *80*, 1691.
- (19) Warshel, A. *Photochem. Photobiol.* **1979**, *30*, 285.
- (20) Warshel, A. Correlation between Structure and Efficiency of Light-Induced Proton Pumps. In *Methods in Enzymology*; Packer, L., Ed.; Academic Press Inc.: London, 1986; Vol. 127, p 578.
- (21) Sham, Y.; Muegge, I.; Warshel, A. *Proteins* **1999**, *36*, 484.
- (22) Warshel, A.; Weiss, R. M. *J. Am. Chem. Soc.* **1980**, *102*, 6218.
- (23) Aqvist, J.; Warshel, A. *Chem. Rev.* **1993**, *93*, 2523.
- (24) Ilan, B.; Tajkhorshid, E.; Schulten, K.; Voth, G. A. *Proteins* **2004**, *55*, 223.
- (25) Murata, K.; Mitsuoka, K.; Hiral, T.; Waltz, T.; Agrel, P.; Heymann, J. B.; Engel, A. *Nature* **2000**, *407*, 599.
- (26) Sansom, M. S. P.; Law, R. J. *Curr. Biol.* **2001**, *11*, R71.
- (27) Tajkhorshid, E.; Nollert, P.; Jensen, M.; Miercke, L.; Stroud, R. M.; Schulten, K. *Science* **2002**, *296*, 525.
- (28) Berendsen, H. J. C. *Science* **2001**, *294*, 2304.
- (29) de Groot, B.; Grubmuller, H. *Science* **2001**, *294*, 2353.
- (30) Kong, Y.; Ma, G. *Proc. Natl. Acad. Sci. U.S.A.* **2001**, *98*, 14345.
- (31) Zeuthen, T. *Trends Biochem. Sci.* **2001**, *26*, 77.
- (32) Law, R. J.; Sansom, M. S. P. *Curr. Biol.* **2002**, *12*, R250.
- (33) de Groot, B. L.; Frigato, T.; Helms, V.; Grubmuller, H. *J. Mol. Biol.* **2003**, *333*, 279.
- (34) Jensen, M. O.; Tajkhorshid, E.; Schulten, K. *Biophys. J.* **2003**, *85*, 2884.
- (35) Yarnell, A. *Chem. Eng. News* **2004**, *82*, 42.
- (36) Warshel, A. *Computer Modeling of Chemical Reactions in Enzymes and Solutions*, 1997 ed.; John Wiley & Sons: New York, 1991.
- (37) Townsley, L. E.; Tucker, W. A.; Sham, S.; Hinton, J. F. *Biochemistry* **2001**, *40*, 11676.
- (38) Štrajbl, M.; Hong, G.; Warshel, A. *J. Phys. Chem. B* **2002**, *106*, 13333.
- (39) Hwang, J. K.; Creighton, S.; King, G.; Whitney, D.; Warshel, A. *J. Chem. Phys.* **1988**, *89*, 859.
- (40) Marcus, R. A. *Annu. Rev. Phys. Chem.* **1964**, *15*, 155.
- (41) Marcus, R. A. *Angew. Chem., Int. Ed. Engl.* **1993**, *32*, 1111.
- (42) McQuarrie, D. A. *Statistical Mechanics*; Harper and Row: New York, 1976.
- (43) Kubo, R.; Toyozawa, Y. *Prog. Theor. Phys.* **1955**, *13*, 160.
- (44) Braun-Sand, S.; Štrajbl, M.; Warshel, A. *Biophys. J.* **2004**, *87*, 2221.
- (45) Hwang, J.-K.; King, G.; Creighton, S.; Warshel, A. *J. Am. Chem. Soc.* **1988**, *110*, 5297.
- (46) King, G.; Warshel, A. *J. Chem. Phys.* **1989**, *91*, 3647.
- (47) Lee, F. S.; Chu, Z. T.; Warshel, A. *J. Comput. Chem.* **1993**, *14*, 161.
- (48) Lee, F. S.; Warshel, A. *J. Chem. Phys.* **1992**, *97*, 3100.
- (49) Warshel, A.; Schlosser, D. W. *Proc. Natl. Acad. Sci. U.S.A.* **1981**, *78*, 5564.
- (50) Alden, R. G.; Parson, W. W.; Chu, Z. T.; Warshel, A. *J. Am. Chem. Soc.* **1995**, *117*, 12284.
- (51) Chu, Z. T.; Villa, J.; Štrajbl, M.; Schutz, C. N.; Shurki, A.; Warshel, A. **2004**.
- (52) Warshel, A.; Sussman, F.; King, G. *Biochemistry* **1986**, *25*, 8368.
- (53) Burykin, A.; Kato, M.; Warshel, A. *Proteins* **2003**, *52*, 412.
- (54) Edwards, S.; Corry, B.; Kuyucak, S.; Chung, S.-H. *Biophys. J.* **2002**, *83*, 1348.
- (55) Mamonov, A. B.; Coalson, R. D.; Nitzan, A.; Kurnikova, M. G. *Biophys. J.* **2003**, *84*, 3646.
- (56) Warshel, A.; Parson, W. W. *Q. Rev. Biophys.* **2001**, *34*, 563.
- (57) Åqvist, J.; Warshel, A. *Biophys. J.* **1989**, *56*, 171.
- (58) Chernyshev, A.; Cukierman, S. *Biophys. J.* **2002**, *82*, 182.
- (59) Burykin, A.; Warshel, A. *Biophys. J.* **2003**, *85*, 3696.
- (60) Chung, S. H.; Allen, T. W.; Hoyles, M.; Kuyucak, S. *Biophys. J.* **1999**, *77*, 2517.
- (61) Cukierman, S. *Biophys. J.* **2000**, *78*, 1825.
- (62) Shurki, A.; Warshel, A. *Adv. Protein Chem.* **2003**, *66*, 249.
- (63) Villa, J.; Warshel, A. *J. Phys. Chem. B* **2001**, *105*, 7887.
- (64) Schmitt, U. W.; Voth, G. A. *J. Phys. Chem. B* **1998**, *102*, 5547.
- (65) Vuilleumier, R.; Borgis, D. *Chem. Phys. Lett.* **1998**, *284*, 71.
- (66) Schutz, C. N.; Warshel, A. *J. Phys. Chem. B* **2004**, *108*, 2066.